🔓 **Open Access**

Narrow-Strip 670 nm Gain-Coupled Distributed Feedback Laser Based on Periodic Anodes Fabricated by I-Line Lithography

Hong Chen
Yongyi Chen
Feng Gao
Li Qin
Chao Chen
Peng Jia
Youwen Huang
Hao Wu
Yongqiang Ning
Lijun Wang

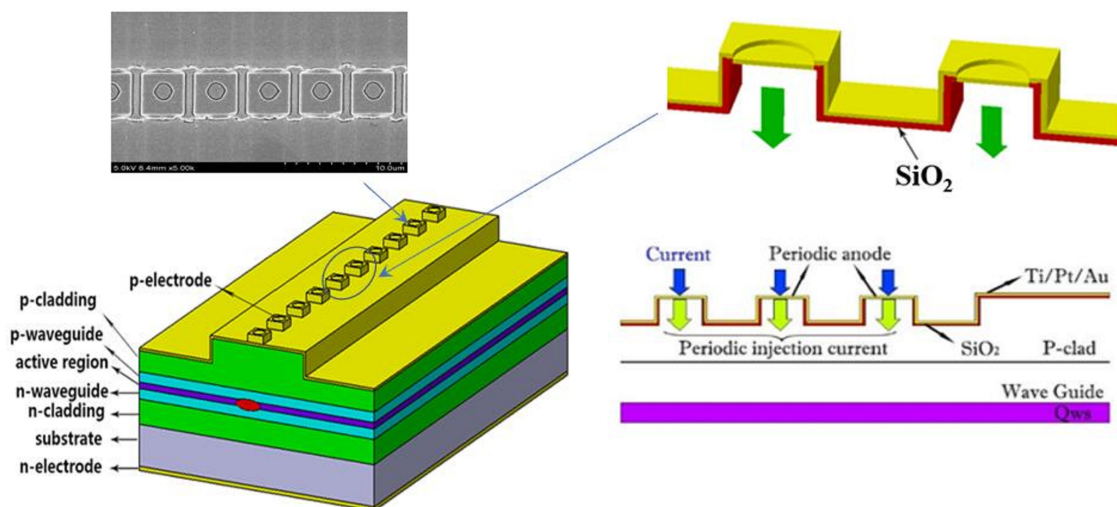# Narrow-Strip 670 nm Gain-Coupled Distributed Feedback Laser Based on Periodic Anodes Fabricated by I-Line Lithography

Hong Chen [ORCID],[1,2] **Yongyi Chen** [ORCID],[1] **Feng Gao** [ORCID],[1] **Li Qin,**[1]
Chao Chen [ORCID],[1] **Peng Jia,**[1] **Youwen Huang,**[1] **Hao Wu** [ORCID],[1]
Yongqiang Ning,[1] **and Lijun Wang**[1]

[1]State Key Laboratory of Luminescence and Applications, Changchun Institute of Optics,
Fine Mechanics and Physics, Chinese Academy of Sciences, Changchun 130033, China
[2]University of Chinese Academy of Sciences, Beijing 100049, China

Abstract: A narrow-strip single-longitudinal-mode gain-coupled distributed feedback semi-
conductor laser with a central wavelength of approximately 670 nm is demonstrated. We
fabricate a novel micro-scale regrowth-free gain-coupled grating with an island-like shape
without nanoscale gratings by i-line lithography only. The maximum output power from
the fiber of the device with butterfly package is 48.1 mW at 100 mA and its slope efficiency
is 0.79 W/A. The laser can be continuously tuned from 670.750 to 670.784 nm with a side-
mode suppression ratio of over 40 dB, covering the absorptive peak of lithium atoms. Our
easily fabricated devices have great potential as light sources in many applications such as
lithium atom detectors.

Index Terms: Semiconductor laser, gain-coupled, distributed-feedback, continuous
tunability.

1. Introduction

Wavelength-tunable 670 nm lasers are well-established laser sources for medical applications
[1], [2], photodynamic therapy devices [3], pump femtosecond Cr3+: LiSAFs [4], laser cooling,
magneto-optical trapping [5], Bose–Einstein condensation with Rubidium and Cesium [5], [6], and,
in particular, lithium atom laser isotope separation [7]–[9]. The 670 nm lasers reported so far include
mainly solid-state lasers, which have extremely low conversion efficiency; dye lasers, which have
very poor stability; and semiconductor lasers, which have high energy conversion efficiency and
stability, small size, light weight, simple structure, relatively low cost, and long life.

So far, the laser sources reported for application in lithium atoms isotope separation generally
consist of a master oscillator power amplifier system, a dye laser, or a solid-state laser. The master
oscillator power amplifier system can be locked to the cross-over peak of the 7Li D2 line [5], but the
external cavity lasers are too large in size, their energy loss is high, and their optical structures are

complicated, resulting in poor reliability and stability [10]. The output power of the reported 670 nm dye laser can reach 1 W [11], but they produce toxic liquid waste that may be harmful to humans. For the reported solid-state laser, which is a diode-pumped 1.3-μm Nd:GdVO4 laser, the intracavity is doubled for more efficient generation of red light and the conversion efficiency is improved compared to previously reported 670-nm solid-state lasers, but they still lack a wavelength tuning mechanism [12]. Although the 670 nm semiconductor diode lasers have great potential, they have been rarely reported. The disadvantage of DBR lasers compared to distributed feedback (DFB) lasers, is the longitudinal mode jump caused by the gain and thermal mismatch of the Bragg reflector when the current injected into the gain portion changes [13]. A red-emitting DFB laser based on a 40th-order surface grating has been presented [14], but the fabrication of its internal devices requires complex and expensive electron beam lithography and secondary epitaxial technology, which significantly limit their large scale production. Furthermore, uniform index-coupled DFB lasers present the intrinsic disadvantage of having two degenerate modes [15].

To solve these problems, a new gain-coupled DFB semiconductor laser based on periodic anodes injection produced by i-lithography is demonstrated in this study. Compared to single-longitudinal-mode lasers with nanoscale grating periods [16], [17], gain-coupled DFB lasers with the proposed surface periodic anodes is more easily fabricated, because it requires only i-line lithography and conventional inductively coupled plasma (ICP) etching instead of complex and expensive fabrication processes. Furthermore, the island-like structures achieve the current injection distribution more easily and are precisely controlled. The periodic surface metal makes contact the island-like insulating trench to create a periodic injection current. The gain contrast is obtained in a quantum well, and a gain coupling mechanism is formed without effective index-coupled effects [18]. Moreover, surface grooves acting as waveguide ridges would lead to more optical loss [19]. A ladder-like shape could reduce the diffusion of current to the sides of the rib and reduce losses [20]. In addition, through such a simple technology, our devices still achieved good performance, and successfully achieved continuous tunability in the range of 34 pm, including the lithium atomic detection peak of 670.776 nm. The output power of the gain-coupled DFB laser is 48.1 mW (larger than the currently reported 670-nm DFB and DBR lasers [14], [21]) with injected current of 100 mA, and slope efficiency of 0.79 W/A at 15 °C (much higher than the currently reported 670-nm Y-branch DBR laser [22] and 670 nm DFB laser [14]). The gain-coupling mechanism provides stable single-longitudinal-mode operation with a 40 dB side mode suppression ratio (SMSR) over a wide current and temperature range (larger than the 670-nm single-mode DBR laser [21]). Owing to secondary epitaxial growth techniques, nanoscale grating fabrication and electron beam lithography are not required; the processing techniques are low cost and simple, and have good application prospects.

2. Structure and Fabrication

The chip structure of the laser was prepared by metal-organic chemical vapor deposition (MOCVD) epitaxial growth and is shown in Table 1. The devices used AlGaInP/GaInP quantum wells (QWs) emitting at 670 nm as the gain material. A schematic diagram of the DFB laser is shown in Fig. 1(a). The fabrication process starts with the deposition of an island-like photoresist layer by i-line lithography. The periodic island-like trenches are insulated with silica, defining the periodic anodes on the unetched periodic regions and the cross-section of the periodic anodes, as shown in Fig. 1(b). A schematic of the periodic current injection operation is shown in Fig 1(c). The silica-insulated periodic island-like trenches and the periodic p-contact electrode form a periodic injection current distribution that causes the gain contrast in the quantum well to form a gain coupling mechanism. Fig. 1(d) shows a scanning electron microscope (SEM) image of the partial structure of the periodic island-like metal p-contact. The finished laser of a butterfly package is shown in Fig. 1(d).

After epitaxial growth by MOCVD, the 4-μm-wide and 3-μm-long periodic island-like structures were fabricated by only i-line lithography on the areas of the wafer on which the ridge waveguides (RWs) will be fabricated. For a conventional DFB laser and a high-order Bragg grating laser, the

TABLE 1

Epitaxial Structures for the 670 nm Chip

Structure	Material	Thickness(nm)
1 Contact	GaAs	200~300
2 P-Clad	AlGaInP	800~1050
3 Wave Guide	AlGaInP	50~150
4 Active Layer	AlGaInP/GaInP	~20
5 Wave Guide	AlGaInP	50~150
6 N-Clad	AlGaInP	800~1000
7 Substrate	GaAs	~350000

index coupling coefficients is kL are greater than 1 [23], [24] and 0.3 [25], respectively. To reduce the index coupling effect induced by the periodic grooves of the island-like, we must design the index coupling coefficient to be small enough to be directly ignored. The theoretical kL is calculated as follows [26], [27]:

$$kL = \frac{L}{\Lambda}\left(\frac{\Delta n}{n_{eff}}\right) \qquad (1)$$

where L is the cavity length of the DFB laser, which is equal to 1 mm; Λ is the period for the 89th island-like grating, which is equal to 9.02 μm; Δn is refractive index change in the waveguide; and n_{eff} is the effective index of the gratings. The effective index n_{eff} of the chip, calculated by COMSOL Multiphysics software, is 3.3235 in the unetched portion and 3.3234 in the etched trench region. Compared to the high-order Bragg grating DFB laser, Λ is much larger (9.02 μm compared to 250 nm of a refractive index-coupled DFB laser [28], [29]) and Δn (0.0001) is smaller. The calculated island-like structure has a kL of only 0.0033, while the high-order multi-longitudinal mode DFB laser's kL is $\sim$0.3 and that of the conventional DFB laser is greater than 1 [23]–[25]. This causes the index-coupled effect to be weak enough to be negligible, ensuring that the device operates under a gain-coupled mechanism.

To better express the effect of the etched gain-coupled island-like structure on the carrier density distribution and the current density distribution in the quantum well, we performed simulations using the commercial software Lastip. Fig. 2(a) shows the difference in the carrier density of the quantum well layer between the structure with and without etched island-like structures. The results show that the carrier density distribution with a peak-to-valley contrast in the quantum well of the periodic anodes device with and without etched island-like structures is approximately 7 × 10^{17} cm^{-3} and 1.5 × 10^{17} cm^{-3}, respectively. As shown in Fig. 2(b), at 1 A, the differences of the peak-to-valley in the current density between the structure with and without etched island-like structures are 3000 A/cm^2 and 700 A/cm^2, respectively. Clearly, the periodic anodes device of the etched island-like structures has a high carrier and current density contrast value in the quantum well layer, which is almost five times larger than that of the pure periodic anode devices. The gain is linearly related to the carrier density [30], and when there is a significant carrier density contrast in the quantum well, a periodic gain contrast is formed, resulting in a gain coupling mechanism. At the same time, the high current density contrast also indicates a high contrast of the optical gain along the cavity.

The period of the island-like structures was set to 9.02 μm to allow the 89th-order Bragg wavelength in the total gain spectrum with a groove length of 6 μm, as shown in Fig. 1(a); the duty cycle was $\sim$33%. Then, the grooves of the island-like structures were etched to 660 nm by an ICP machine. After the formation of the island-like structures, the 6-μm-wide RWs were patterned by i-line lithography and etched to 900 nm using an inductively coupled plasma etcher on either sides of the island-like structure. This layer forms a lateral optical confinement structure that greatly reduces the effect of lateral groove loss. A 300-nm-thick silica layer was then deposited on top of the
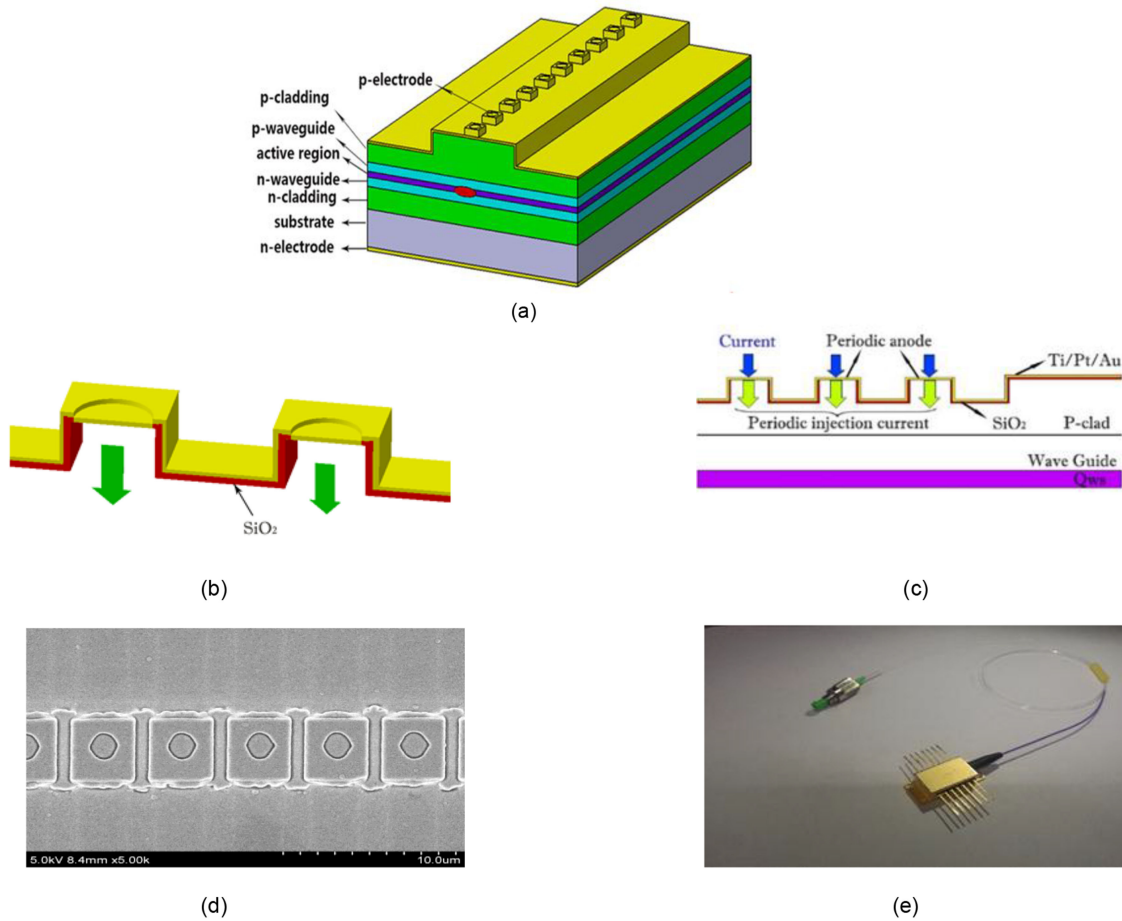
Fig. 1. Device Schematic. (a) Structure of the gain-coupled DFB laser based on periodic surface anodes, (b) cross-section of the periodic anodes, (c) periodic injection current operation, (d) SEM image of the p-electrodes partial structure, and (e) picture of the butterfly packaged device.
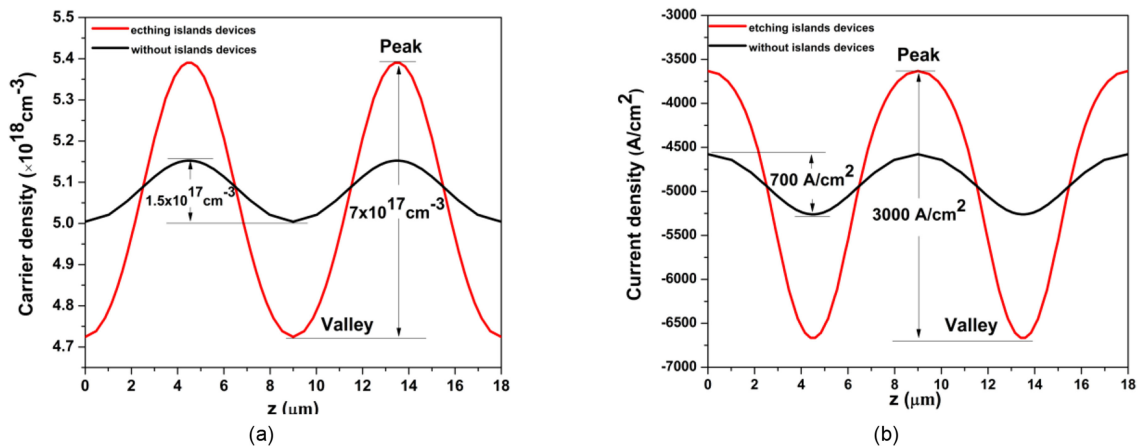

Fig. 2. (a) One-dimensional carrier density distribution in the quantum well for the etched island-like devices and pure periodic anode devices without etched island-like structures. (b) One-dimensional current density distribution in the quantum well for the etched island-like devices and pure periodic anode devices without etching island-like structures.

epitaxy by plasma enhanced chemical vapor deposition for electrical insulation, i-line lithography was performed to pattern the periodic current injection window with 2 μm^2 (as shown in Fig. 1(a)) on the island-like structure, and dry etching was performed to form the anode grooves. The injection current was transmitted through the periodic anodes, resulting in a periodic carrier density distribution in the quantum well and a periodic gain contrast in the quantum well [30]. Compared with the previously reported 670 nm lasers, our proposed gain-coupled DFB laser is simple in structure, requiring only i-line lithography and basic ICP etching, which results in higher stability, easier fabrication, and thus, feasible mass production.

A surface periodic metal p-contact was then formed by magnetron sputtering, followed by p-side Ti-Pt-Au contact metal deposition, substrate thinning and polishing, and n-side Au-Ge-Ni/Au metal deposition. Finally, the chips were cut to 1 mm in length and the two facets of the laser were coated with an antireflection film (with approximately 0.5% reflectivity) on one face and a high-reflection film (with approximately 99% reflectivity) on the other.

The devices were mounted p-side up on simple COS-mount heat sinks. The COS module and the thermo electric cooler (TEC) heat sink were integrated into the butterfly shell and connected to a TEC temperature control device to maintain a constant temperature for testing.

3. Results and Discussion

The power-current-voltage characteristics at continuous-wave (CW) operation at 15 °C are shown in Fig. 3. A schematic diagram of the current injection is shown in Fig. 2(c). During the testing process, we used the bevel test to avoid the influence of external light. Fig. 3(a) shows that the threshold current of the FP laser at 15 °C is 10 mA with a slope efficiency of 1 W/A. Fig. 3(b) shows a typical electro-optical characteristic of a DFB laser. As shown in the figure, compared with the FP laser, the threshold current of the gain-coupled DFB laser increases to 40 mA and, at the same time, the slope efficiency drops down to 0.79 W/A (much lower than the previously reported 670-nm Y-branch DBR laser [22] and 670-nm DFB laser [14]). The output powers of the FP and gain-coupled DFB lasers with an injected current of 100 mA are 89.2 mW and 48.1 mW, respectively (larger than the previously reported 670 nm DFB and DBR lasers [14], [21]). These are slightly lower for the DFB laser than the FP laser because the former operates in a single-longitudinal mode. The spectrum of the gain-coupled DFB laser with an injection current of 100 mA and an operating temperature of 15 °C is shown in Fig. 4. As shown in Fig. 3(b), there exists a kink in the P-I curve, which results from the mode-hopping of the lasers. This mode hopping can be attributed to self-heating effects and to a shift of the gain peak across the Bragg wavelength [14].

The CW spectrum characteristics were measured with a YOKOGAWA AQ6370C spectrum analyzer. Fig. 5(a) shows the variations in the center wavelength of the gain-coupled DFB laser based on the periodic anodes with different currents at operating temperature of 15 °C. It is clearly shown that the wavelength red shifts as the injection current increases. When the injection current increases from 65 to 74 mA, the peak wavelength shifts from 670.750 to 670.784 nm, respectively, at a rate of ~3.8 pm/mA and the wavelength tuning reaches 34 pm. When the injection current is 73 mA, the center wavelength peak is 670.776 nm. Fig. 5(b) shows that the device achieved single-longitudinal-mode operation by the periodic injection of current with a SMSR of more than 40 dB (larger than the lasers with nanoscale [31], [32]) at the peak of 670.776 nm. Therefore, our proposed 670 nm DFB laser with gain-coupling mechanism has successfully achieved continuous tunability in the vicinity of the main peak at 670.776 nm of the lithium atom detection. For the other two lithium isotopes, the position of this tuning center is slightly shifted, but the tuning range obtained is sufficient. Thus, we will continue to optimize our device structure for a more comprehensive application in lithium atoms detection.

The tunability of the device's wavelength at different temperatures was tested. Fig. 6 shows the peak wavelengths and SMSR of the gain-coupled DFB laser operating at different temperatures with an injection current of 75 mA. When the operating temperature was increased from 11 °C to 21 °C, the center wavelength shifted at a rate of ~0.187 nm/°C (much better than ordinary DFB lasers [33]). The blue curve in Fig. 6 represents the SMSR curve corresponding to the peak wavelength.
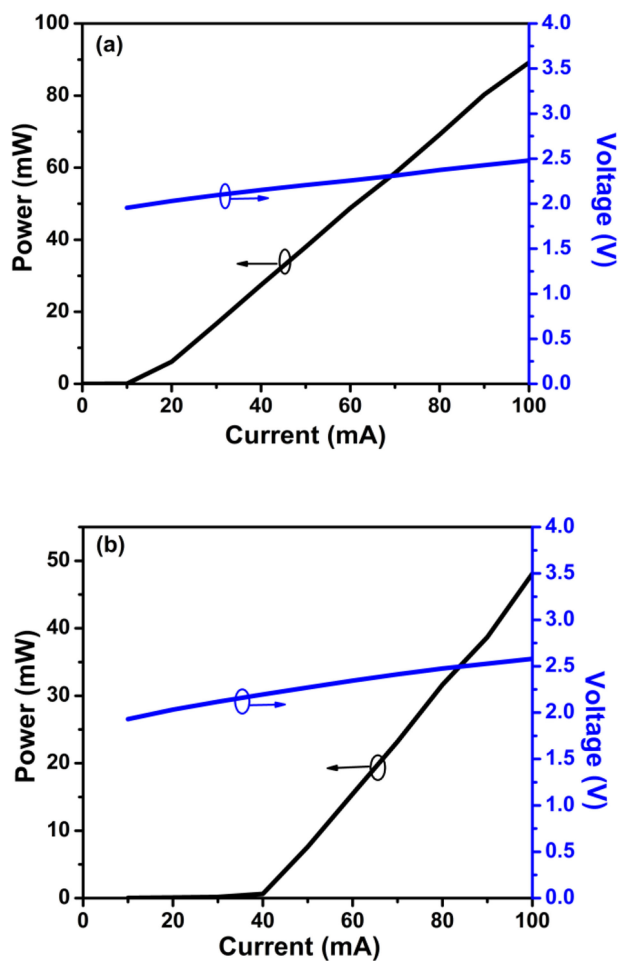
Fig. 3. CW power-current-voltage characteristics of the (a) FP laser and (b) gain-coupled DFB laser at operating temperature of 15 °C.
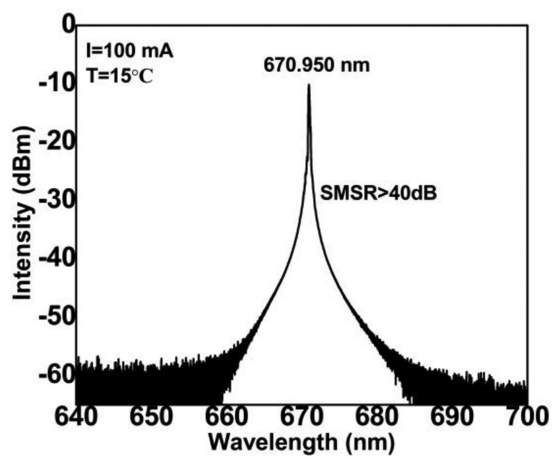

Fig. 4. The spectrum of the gain-coupled DFB laser with an injection current of 100 mA and an operating temperature of 15 °C.
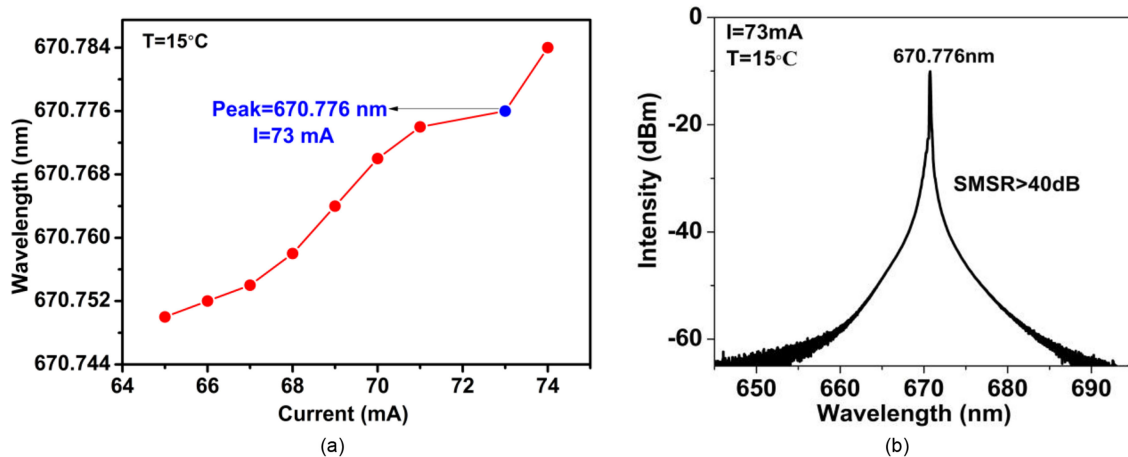
Fig. 5. (a) Center wavelength variations of the DFB laser with different currents at operating temperature of 15 °C. (b) Measured emission spectrum characteristics (I = 73 mA) of the gain-coupled DFB lasers at 15 °C.
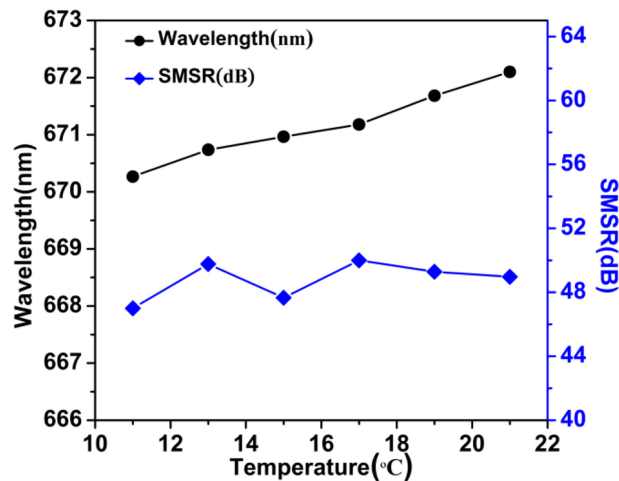

Fig. 6. Center wavelength and SMSR of the gain-coupled DFB laser with different operating temperatures at an injection current of 75 mA (blue squares: SMSR; black circles: center wavelength).

it can be seen from the figure that the minimum SMSR, corresponding to the peak wavelength of 670.266 nm at 11 °C, is 47 dB, and the maximum SMSR, corresponding to the peak wavelength of 672.1 nm at 21 °C, is 50 dB. This clearly shows that the single-longitudinal-mode operation is stable over a wide temperature range.

Fig. 7 shows the emission spectrum characteristics of the FP and gain-coupled DFB lasers at different temperatures when the injection current is 75 mA. The FP lasers that were fabricated on the same chip for comparison worked at multi-longitudinal modes, as shown in Fig. 7(a). However, Fig. 7(b) shows that the gain-coupled DFB laser achieves a stable single-longitudinal-mode emission with SMSR of more than 40 dB. Because the periodic injection current could introduce a gain coupling mechanism, the additional modes were filtered out and single-longitudinal-mode operation was achieved.
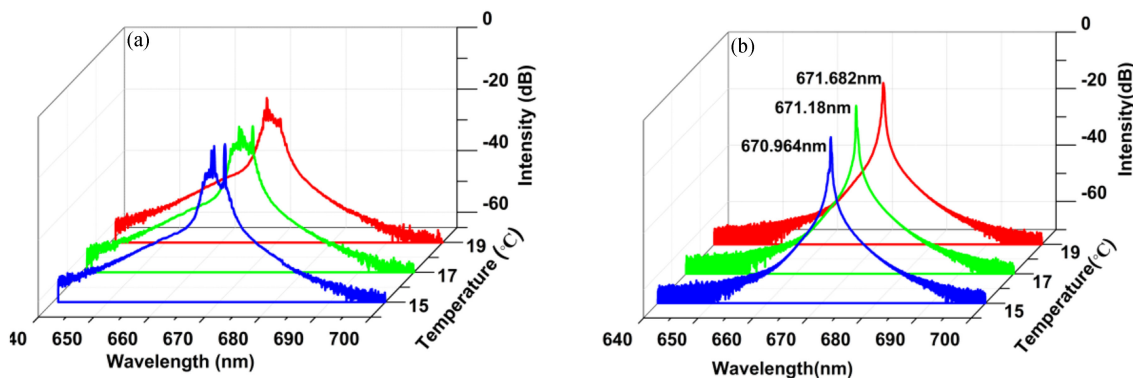
Fig. 7. Measured emission spectrum characteristics (I = 75 mA) of the (a) FP lasers and (b) gain-coupled DFB lasers at different temperatures.

4. Conclusions

A narrow-strip single-longitudinal-mode gain-coupled DFB semiconductor laser based on periodic anodes with a center wavelength of approximately 670 nm was demonstrated. We fabricated a novel micro-scale regrowth-free gain-coupled grating with island-like shape without nanoscale gratings by i-line lithography only. The silica-insulated periodic island-like trench and the periodic p-contact electrode caused a periodic injection current distribution, which resulted in the gain contrast in the quantum well, forming a gain coupling mechanism. Despite the simplicity of the fabrication, our device achieved good performance; it successfully achieved continuous tunability in the tuning range of 34 pm and detected the lithium peak of 670.776 nm. The output power of the gain-coupled DFB laser reached 48.1 mW with an injected current of 100 mA, and the slope efficiency was 0.79 W/A. The wavelength peak shifted with current and temperature at rates of ∼3.8 pm/mA and ∼0.187 nm/°C, respectively, which are better than those of ordinary DFB lasers. The gain-coupling mechanism provides stable single-longitudinal-mode operation with a SMSR of more than 40 dB over wide current and temperature ranges. Secondary epitaxial growth techniques, nanoscale gratings fabrication, electron beam lithography, and step lithography are not required. The processing techniques are low cost and simple. We believe that the proposed conceptual design and fabrication methods have great potential, especially in the 6xx nm wavelength range.

References

[1] G. Hatakoshi *et al.*, "High-power InGaAlP laser diodes for high-density optical recording," *Jpn. J. Appl. Phys.*, vol. 31, no. 2B, pp. 501–507, 2014.
[2] T. Siegle *et al.*, "Photonic molecules with a tunable inter-cavity gap," *Light, Sci. Appl.*, vol. 6, no. 3, 2016, Art. no. e16224.
[3] K. Masumoto *et al.*, "Tissue distribution of a new photosensitizer ATX-S10Na(II) and effect of a diode laser (670 nm) in photodynamic therapy," *Lasers Med. Sci.*, vol. 18, no. 4, pp. 227–227, 2004.
[4] J. Fricke *et al.*, "20000 h reliable operation of 100 μm stripe width 650 nm broad area lasers at more than 1.1 W output power," *Semicond. Sci. Technol.*, vol. 26, no. 10, 2011, Art. no. 105011.
[5] R. Häring *et al.*, "670 nm semiconductor lasers for lithium spectroscopy with 1W," *Proc. SPIE*, vol. 6485, 2007, Art. no. 648516.
[6] T. D. F. Hof and H. J. Jänsch, "Application of diode lasers as a spectroscopic tool at 670 nm," *Opt. Commun.*, vol. 124, nos. 3/4, pp. 283–286, 1996.
[7] I. E. Olivares and I. A. González, "Diode laser absorption spectroscopy of lithium isotopes," *Appl. Phys. B*, vol. 122, no. 10, pp. 252-1–252-7, 2016.
[8] I. E. Olivares *et al.*, "Lithium isotope separation with tunable diode lasers," *Appl. Opt.*, vol. 41, no. 15, pp. 2973–2977, 2002.
[9] T. Arisawa, Y. Maruyama, Y. Suzuki, and K. Shiba, "Lithium isotope separation by laser," *Appl. Phys. B*, vol. 28, no. 1, pp. 73–76, 1982.
[10] M. Chi *et al.*, "Tunable high-power narrow-linewidth semiconductor laser based on an external-cavity tapered amplifier at 670 nm," in *Proc. Conf. Lasers Electro Opt. Pacific Rim Conf. Lasers Electro-Opt.*, 2009, pp. 1–2.

[11] W. J. Kessler and S. J. Davis, "Continuous-wave visible diode-pumped dye laser," *Proc. SPIE*, vol. 2115, pp. 204–212, 1994.

[12] A. Agnesi *et al.*, "High-brightness 2.4-W continuous-wave Nd:GdVO4 laser at 670 nm," *Opt. Lett.*, vol. 29, no. 1, pp. 56–58, 2004.

[13] M. Radziunas *et al.*, "Mode transitions in distributed Bragg reflector semiconductor lasers: Experiments, simulations and analysis," *J. Phys. B, Atomic, Mol. Opt. Phys.*, vol. 44, no. 10, 2011, Art. no. 105401.

[14] J. Fricke *et al.*, "Red-emitting distributed-feedback ridge-waveguide laser based on high-order surface grating," *Electron. Lett.*, vol. 54, no. 9, pp. 582–583, 2018.

[15] H. Kogelnik and C. V. Shank, "Coupled-wave theory of distributed feedback lasers," *J. Appl. Phys.*, vol. 43, pp. 2327–2335, 1972.

[16] M. Nawrocka *et al.*, "Widely tunable six-section semiconductor laser based on etched slots," *Opt. Exp.*, vol. 22, no. 16, p. 18949–18957, 2014.

[17] R. J. Guo *et al.*, "Multisection DFB tunable laser based on REC technique and tuning by injection current," *IEEE Photon. J.*, vol. 8, no. 4, Aug. 2016, Art. no. 1503007.

[18] D. Kais, B. Abdessamad, Z. Jessica, H. Karin, and T. J. Hall, "Narrow linewidth two-electrode 1560 nm laterally coupled distributed feedback lasers with third-order surface etched gratings," *Opt. Exp.*, vol. 22, no. 16, pp. 19087–19097, 2014.

[19] G. Feng *et al.*, "Narrow-strip single-longitudinal-mode laser based on periodic anodes defined by i-line lithography," *IEEE Photon. J.*, vol. 10, no. 2, Apr. 2018, Art. no. 1501910.

[20] T. Wang *et al.*, "Injection-insensitive lateral divergence in broad-area diode lasers achieved by spatial current modulation," *Appl. Phys. Exp.*, vol. 9, no., 11, 2016, Art. no. 112102.

[21] O. Pezeshki and J. S. Osinki, H. Zhao, A. Mathur, and T. L. Koch, "GaInP/AlGaInP 670 nm single mode DBR laser," *Electron. Lett.*, vol. 32, no. 24, pp. 2241–2243, 2002.

[22] M. Maiwald *et al.*, "Dual-wavelength monolithic Y-branch distributed Bragg reflection diode laser at 671 nm suitable for shifted excitation Raman difference spectroscopy," *Laser Photon. Rev.*, vol. 7, no. 4, pp. L30–L33, 2013.

[23] M. I. Sargent, W. Swantner, and J. Thomas, "Theory of a distributed feedback laser," *IEEE J. Quantum Electron.*, vol. 16, no. 4, pp. 465–472, Apr. 1980.

[24] M. Kanskar *et al.*, "53% wallplug efficiency 975nm distributed feedback broad area laser," *Electron. Lett.*, vol. 42, no. 25, pp. 1455–1457, Dec. 2006.

[25] J. Decker, "Narrow stripe broad area lasers with high order distributed feedback surface gratings," *IEEE Photon. Technol. Lett.*, vol. 26, no. 8, pp. 829–832, Apr. 2014.

[26] S. L. Chuang, *Physics of Photonic Devices*. Hoboken, NJ, USA: Wiley, 2009.

[27] M. Osinski, "Diode lasers and photonic integrated circuits," *Opt. Eng.*, vol. 36, no. 2, pp. 613–618, 1997.

[28] Y. Shi, S. Li, R. Guo, R. Liu, Y. Zhou, and X. Chen, "A novel concavely apodized DFB semiconductor laser using common holographic exposure," *Opt. Exp.*, vol. 21, no. 13, pp. 16022–16028, 2013.

[29] J. Li *et al.*, "Experimental demonstration of distributed feedback semiconductor lasers based on reconstruction-equivalent-chirp technology," *Opt. Exp.*, vol. 17, no. 7, pp. 5240–5245, 2009.

[30] B. W. Hakki, "Carrier and gain spatial profiles in GaAs stripe geometry lasers," *J. Appl. Phys.*, vol. 44, 1973, Art. no. 5021.

[31] L. Liu, H. Qu, Y. Wang, Y. Liu, Y. Zhang, and W. Zheng, "High-brightness single-mode double-tapered laser diodes with laterally coupled high-order surface grating," *Opt. Lett.*, vol. 39, no. 11, pp. 3231–3234, 2014.

[32] T. N. Vu, A. Klehr, B. Sumpf, H. Wenzel, G. Erbert, and G. Trankle, "Tunable 975 nm nanosecond diode-laser-based "master-oscillator power-amplifier system with 16.3 W peak power and narrow spectral linewidth below 10 pm," *Opt. Lett.*, vol. 39, no. 17, pp. 5138–5141, 2014.

[33] Y. Zheng, T. Sekine, T. Kurita, Y. Kato, and T. Kawashima, "Continuous-wave dual-wavelength operation of a distributed feedback laser diode with an external cavity using a volume Bragg grating," *Jpn. J. Appl. Phys.*, vol. 57, 2018, Art. no. 030307.